Journal of Geophysical Research: Solid Earth

Supporting Information for

Wall Fracturing versus Mechanical Instability as competing intrusion Mechanisms of Dikes: Insights from Laboratory Experiments

Uddalak Biswas[1], Atin Kumar Mitra[1], and Nibir Mandal[2]

[1]Structural Geology Lab., Department of Earth Sciences, Indian Institute of Engineering Science and Technology, Shibpur, Howrah 711103, West Bengal, India
[2]Department of Geological Sciences, Jadavpur University, Kolkata 700032, India

Corresponding author: Uddalak Biswas (uddalakbiswashriku@gmail.com)

Introduction

This is the supporting information used to develop the present manuscript.

Regional structural evolution S1.

On a regional scale, the rocks of CGGC suffer ductile deformations (Sanyal & Sengupta, 2020) because of the overall tectonic movement of the terrain from the north to south direction. The deformation is denoted by the development of penetrative fabric in the country rock. In places, fabric further gets folded by later deformation. The area is intruded by pegmatites that show cross-cutting relation with the main fabric and later-stage folds.

Field documentation S2

To study the pegmatisation process and the geometrical variation of intrusive granite, we prepared high resolution (scale in order of 1:100) plain paper map in two selective locations of south-east CGGC (Figure. 8a). The locations were Balakdih (23°12.8264´N, 86°31.029´E), and Chakultar (23°14.258´N, 86°21.764´E), Purulia district, West Bengal. Both locations have an excellent exposure of several generations' granite pegmatite into the granite gneiss.

The study areas show gneissic foliation defined by the separate alternating felsic quartzo-felspathic and mafic biotite or amphibolite banding. This outcrop also consists of several emplacements of pegmatites. Some of them are almost parallel to, and some are crosscutting the major gneissic foliation (Figure 8b). One dominant set of thick (thickness varies from 1.5m to ~3m) pegmatites emplaced along the foliation. These sets of pegmatites show bifurcation and anastomosing nature in places. In some places of the outcrop, country rocks occur as enclaves within the pegmatite (Figure 8c). There is also a set of thin pegmatite (thickness is ~1.2cm), which is at a low angle with the general foliation, shows crosscutting relationship with the previous one, and the third sets of pegmatite are present at a very high angle with major gneissic foliation thickness varying from 30cm to ~4m, crosscut all the other foliations.

Complex rheological properties of the model material S3.

The choice of the model material is very much crucial to simulate the natural process efficiently. The correct choice of the model material needs proper scaling. To scale a model accurately, it should be

geometrically, kinematically, and dynamically similar to its natural counterpart (Hubbert, 1937; Ramberg, 1981). Most of the previous workers used pure endmember rheology for the host. However, the crust of the earth is not purely viscous or elastic, or plastic. Rather, it behaves visco-elasto-plastically and accommodates the incoming fluid by hybrid deformation (Rubin, 1993; Vachon & Hieronymus, 2016; Scheibert et al., 2017).

That is why we choose two complex rheological materials to represent the host. The first material we choose is Ultrasound Transmission Gel (*USTG*), which is readily available commercially. We bought a batch of *USTG* from the market so that the composition remains the same. The *USTG* we use is mainly composed of Carbopol powder and water. Carbopol gel is nowadays a widely used model material to mimic crustal rheology, specifically the visco-elasto-plastic nature of the lower crustal rheology (Reber et al., 2020). Semi-brittle deformation processes have been modeled using Carbopol gel (Birren & Reber, 2019; Reber et al., 2015). Having these optimum rheological properties, the transparency of the gel made it perfect for the observation of the ongoing emplacement process in 3D. In gel form, it behaves like a non-linear power-law fluid following the Herschel-Bulkley model for stress-strain rate approximation.

$$\sigma = \sigma_y + K_v \dot{\varepsilon}^n \text{ — Eqn. (S1)}$$

The stress σ depends on the strain rate $\dot{\varepsilon}$, the flow index n, the consistency K_v, and the yield stress σ_y. The Carbopol gel is basically a combination of elastoplastic grains and fluid on a micro-scale (Oppong & de Bruyn, 2011; Piau, 2007; Reber et al., 2020; Shafiei et al., 2018).

The bulk viscosity of the gel depends on the pH of the water. Below the yield stress, Carbopol gel (*USTG*) deforms elastically, and beyond the yield stress, it deforms viscously. The yield stress can be changed by changing the water and Carbopol powder ratio in *USTG*

. It can also be considered a composite material with elastoplastic and viscous behavior in a separate range of strains.

We use gel wax which is composed of mineral oil and hydrocarbon-based polymer. Gel wax is a Gelatine like material, which is widely used in the analog experiments of dyke and sill emplacement (e.g., Canon-Tapia and Merle, 2006; Hyndman & Alt, 1987; Kervyn et al., 2009; Rivalta et al., 2005). The rheology of the gel wax resembles upper crustal visco-elastic behavior. The rheology of the gel wax can be described by a combination of spring and dashpot.

The rheology of the *USTG* depends on the water, the Carbopol powder ratio, and the pH of the water. On the other hand, the rheology of the Gel wax depends on the concentration of the mineral oil. So, to identify the true nature of these materials used in our experiment, we tested them in Anton Paar Modular Compact Rheometer 302e.

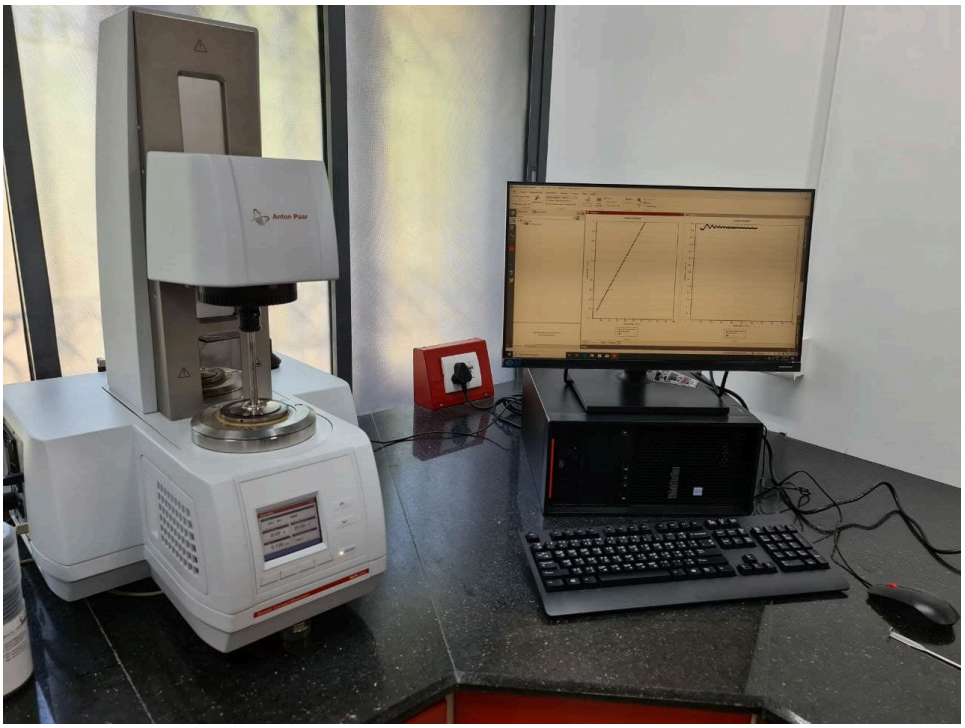

Figure S1. Laboratory setup (Anton Paar Modular Compact Rheometer 302e) used for the rheological tests of experimental model materials.

As the overall property of these two materials was known as visco-elasto-plastic and visco-elastic, we performed oscillatory tests, also known as Dynamic Mechanical Analysis which is ideal for this type of material. We perform two types of oscillatory tests a) Amplitude sweeps and b) Frequency sweeps.

a) Amplitude sweeps:

These are the oscillatory tests where the amplitude will vary, keeping the frequency constant. For controlled shear strain, $\gamma(t) = \gamma_A \cdot \sin\omega t$ where, γ_A= shear strain amplitude (in %) = $\gamma_A(t)$, ω= angular frequency (s^{-1}) = constant, t= time. (Fig. S2)

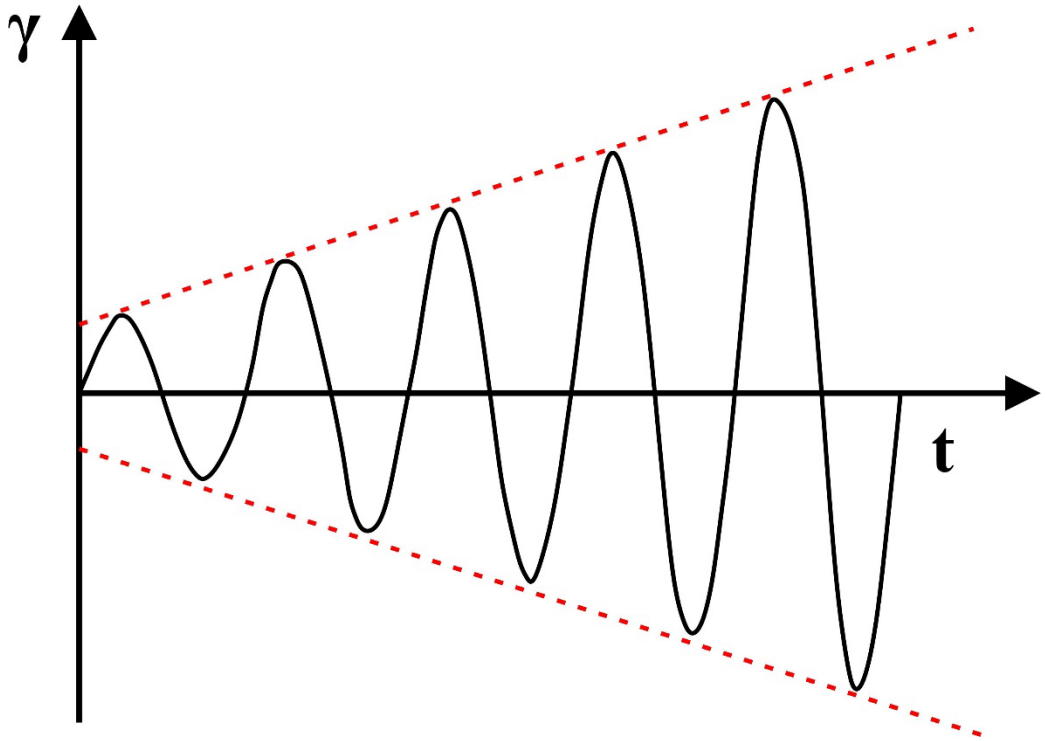

Figure S2. Oscillating strain (g) imposed in the rheometer at a constant angular frequency same (after Mezger, 2014) in the amplitude test of rheology.

Similarly, for controlled shear stress, $\tau(t) = \tau_A \cdot \sin\omega t$ where τ_A = shear stress amplitude (in %) = $\tau_A(t)$, ω= angular frequency (s^{-1}) = constant, t= time.

The results of the amplitude sweep tests produce the variation of storage modulus (G') and loss modulus (G") with respect to time. The storage modulus or G' values are measures of the deformation energy stored by the sample during the shear process, which is the representation of the elastic behavior of a material. On the other hand, the loss modulus or G" values are the measures of the lost deformation energy and are the representation of the viscous behavior of the material (Mezger, 2014). From these results, we can calculate the

complex shear modulus (G^*), which can be imagined as the rigidity of the material, i.e., t total viscoelastic resistance against deformation.

$$|G^*| = \sqrt{(G')^2 + (G'')^2} \quad \text{—Eqn. (S2)}$$

G* consist of both elastic (G′) and viscous (G″) part representing complete viscoelastic behavior. Depending upon the G′ and G″ values, the rheology of the material can be explained as mentioned in the following Table (after Mezger, 2014):

Ideal viscous flow behavior of liquid	Viscoelastic behavior of liquid	Viscoelastic behavior with 50/50 ratio of viscous and elastic properties	Viscoelastic behavior of gel/solid	Ideal elastic behavior of solids
$G' \rightarrow 0$	$G'' > G'$	$G' = G''$	$G' > G''$	$G'' \rightarrow 0$

Table S1. Shear modulus properties of major rheological types of materials. G′: complex elastic shear modulus; G″: viscous loss shear modulus.

The log-log plot of G′ and G″ concerning strain amplitude shows almost linear behavior for lower values of strain amplitude up to a particular limiting value (γ_L). Then both deals start to decline at different rates. G′ value decline at a higher rate so that it crosses over for gel-like material (G′ > G″) with further increase in strain (Fig. S3). The range in which the G′ and G″ maintain linear values is called Linear Visco-Elastic Range (LVER).

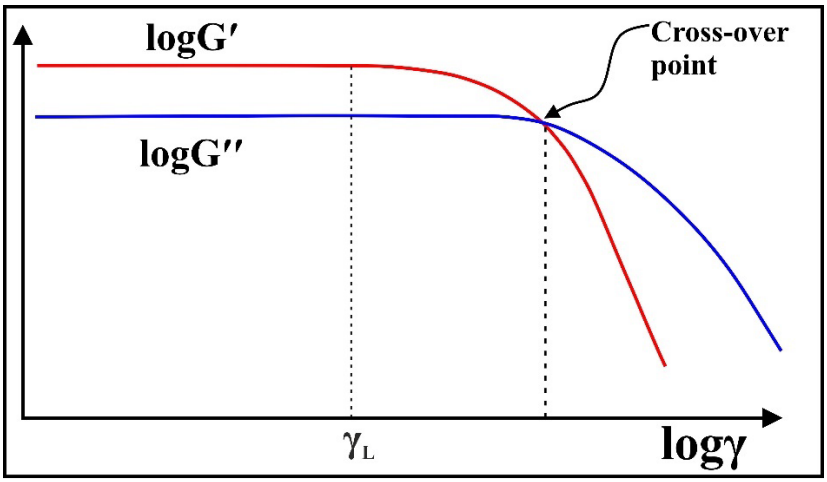

Figure S3. Log-log plots of strain sweep-test data for storage and loss modulus for gel-like materials and viscoelastic solids (after Mezger, 2014).

Similarly, in lower stress values, the G′ and G″ plots look similar to plots with respect to strain. The point at which the LVER ends is called the yield point or yield stress (τ_y), and the cross-over point (for gel-like material, i.e., G′ > G″) is called the flow point or flow stress (τ_f). So, for a gel-like solid in LVER (G′ > G″), it behaves like a solid, then after the yield point, it starts to creep internally until the flow point (G′ = G″) and finally, after crossing the flow point (G″ > G′), it flows as a whole like a viscous fluid (Fig. S4).

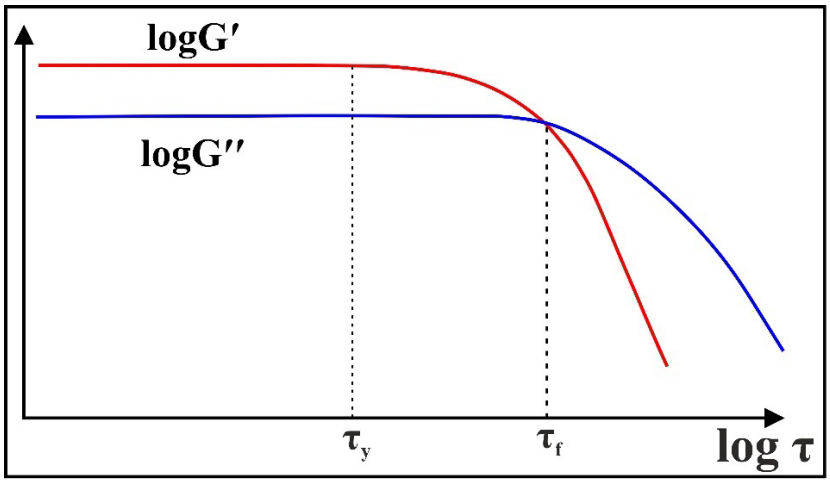

Figure S4. Log-log plots of stress sweep test data for storage and loss moduli for gel-like material and viscoelastic solid (after Mezger, 2014).

For some cross-linked polymer after LVER, the value of G″ don't decline with increasing deformation. Rather it starts to rise and reaches a peak value, finally declining (Fig. S5). Increasing G′-values indicate an increasing portion of deformation energy which is used up already before the final breakdown of the internal superstructure occurs, to irreversibly deform at first only parts of the latter (Mezger, 2014). This may occur due to relative motion between the molecules, flexible end-pieces of chains and side chains, long network bridges, mobile single particles, agglomerates, or superstructures which are not linked or otherwise fixed in the network.

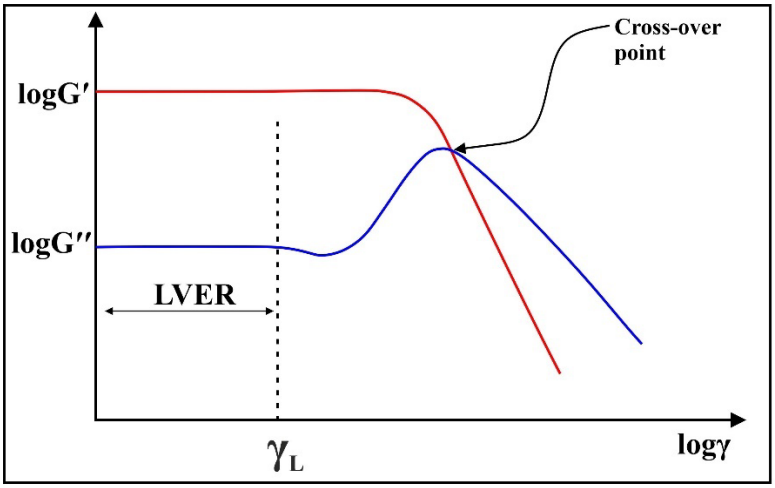

Figure S5. Strain amplitude sweep of a sample test showing a G″-peak (after Mezger, 2014).

b) Frequency sweeps:

These are types of oscillatory tests where the amplitude of the deformation remains the same, but the frequency changes with time. For tests with controlled shear strain: $\gamma(t) = \gamma_A \cdot \sin\omega t$ with γ_A = const and a variable angular frequency $\omega = \omega(t)$, only the period of time for each one of the oscillation cycles are increasing or decreasing continuously, respectively (frequency) (Fig. S6).

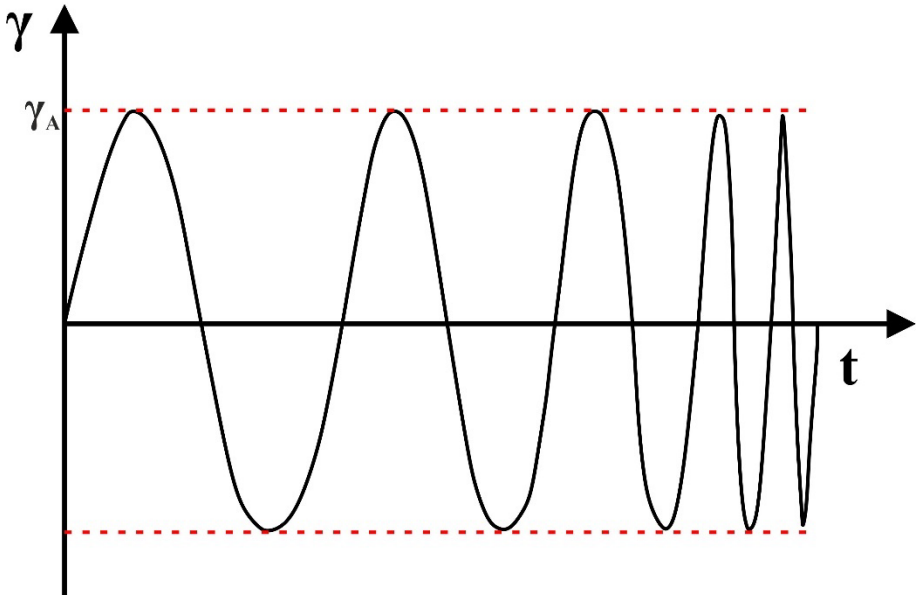

Figure S6. Strain test with varying angular frequency with time, keeping a constant strain amplitude (after Mezger, 2014)

Similarly, for tests with controlled shear stress: $\tau(t) = \tau_A \cdot \sin\omega t$, with τ_A = const and $\omega = \omega(t)$.

Results:

Gel Wax:

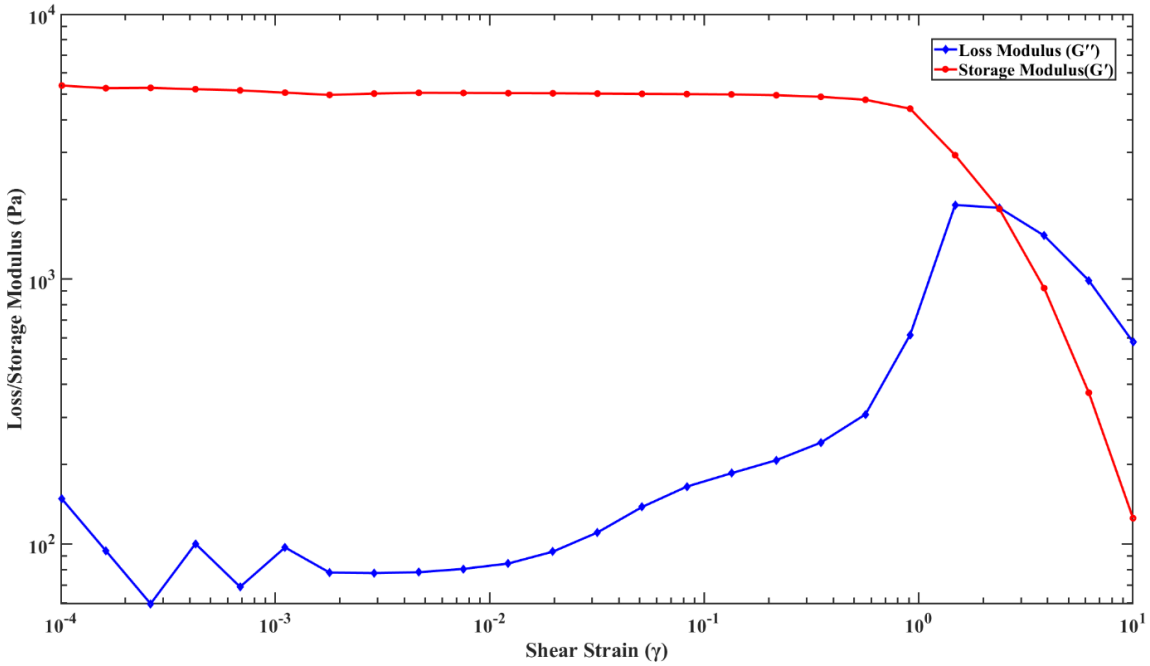

Figure S7. Results of strain sweep tests run on gel Wax. Note that G′ (storage modulus) > G″ (loss modulus), implying its viscoelastic solid rheology.

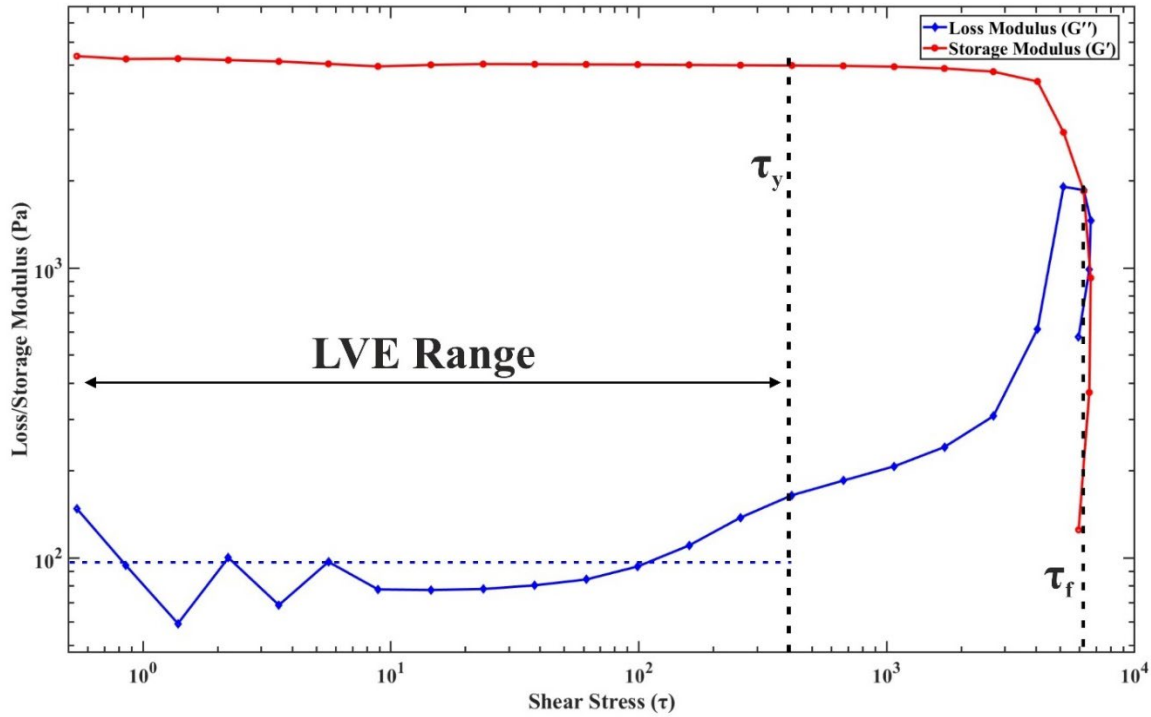

Figure S8. Results of stress sweep tests on gel wax. Yield stress (τ_f): 499 Pa

USTG:

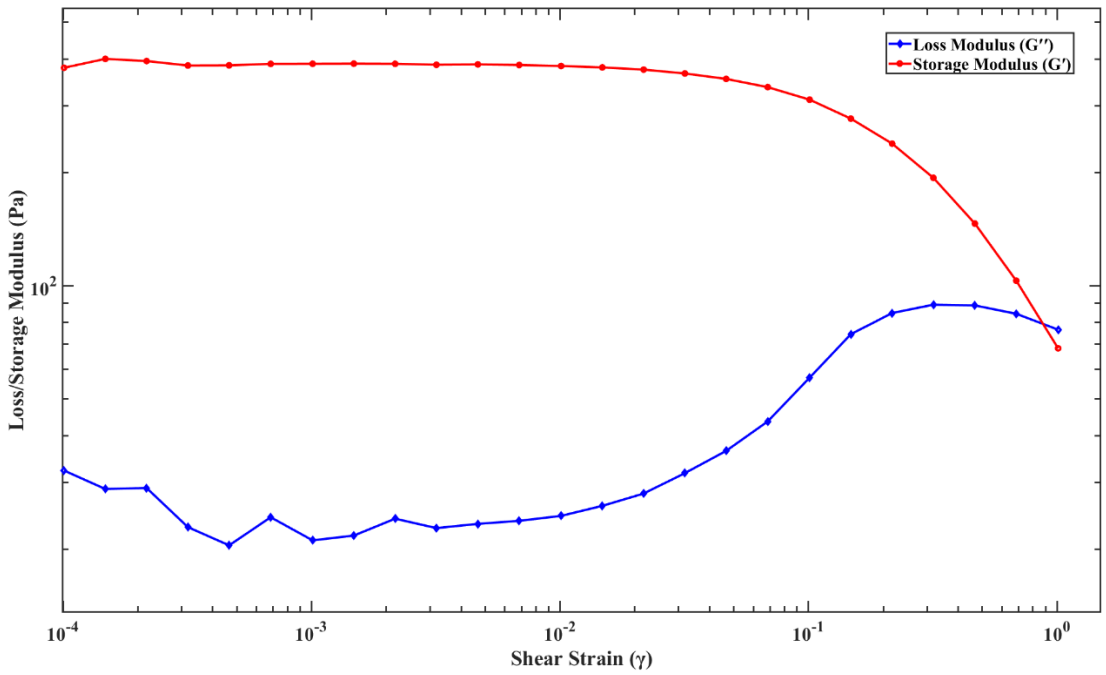

Figure S9. Strain sweep test result for *USTG*.

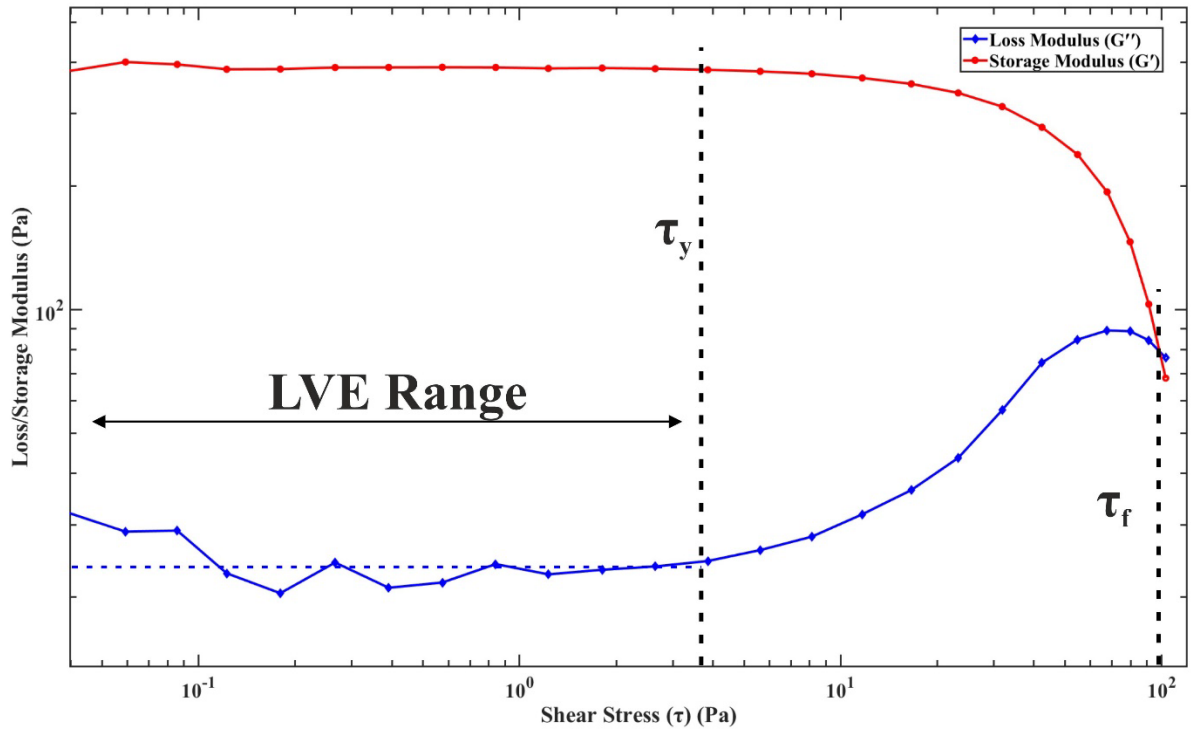

Figure S10. Stress sweep test result for *USTG*. Yield stress (τ_f): 3.84 Pa

We used commercial hair oil as an intruded melt during the experiment. The hair oil assumes to be a Newtonian fluid. So, we perform a rotational flow test in the Rheometer to measure the viscosity of the hair oil. The result is showing linear stress versus strain rate curve, and no change in viscosity with strain rate implies it is a Newtonian fluid.

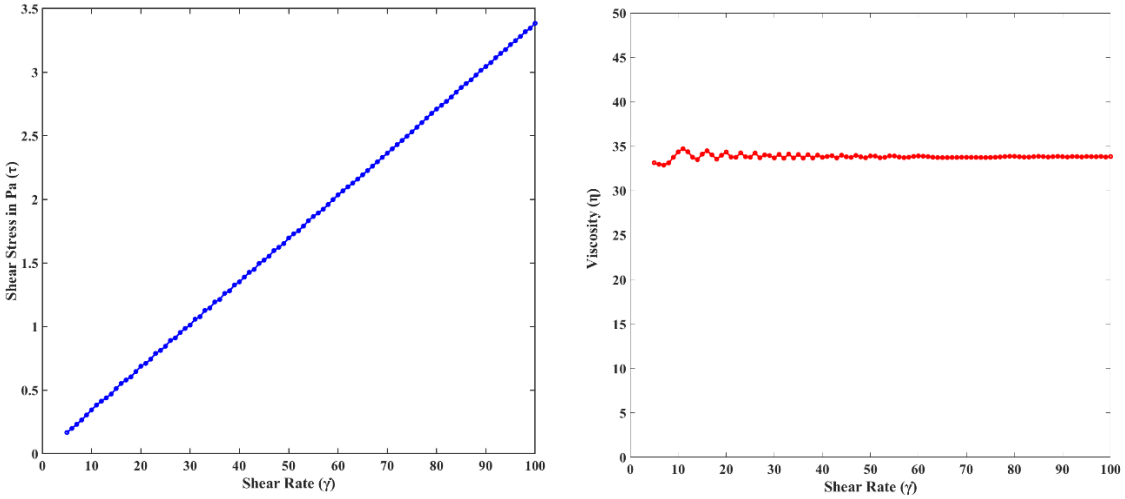

Figure S11. Result of rotation tests on hair oil used as analog magma liquid in the laboratory experiments. *Left*: Plots of stress versus strain rate, showing a typical linear curve for Newtonian viscous rheology. *Right:* Strain-rate independent viscosity (η in mPa) of the liquid.

Method of 2-D fractal dimension calculation S4.

We performed a fractal analysis of the shear surface roughness observed in both field and laboratory models. A fractal set of objects can be defined as

$$N = \frac{C}{r^D} \quad \text{—Eqn. (S3)}$$

where N is the number of objects with linear dimension r, C is the proportionality constant, and D is the fractal dimension. In equation (1), N holds a power law relation with r, and their distribution on a log space shows essentially a linear regression.

The boundaries between the host and the intruded liquid were drawn for both the experimental models and the field photograph using MATLAB. The image of the boundaries is then converted to

a binary image. The 2D fractal dimensions were calculated using "***boxcount***" function in the MATLAB environment following the method described in the following link—

http://www.fast.u-psud.fr/~moisy/ml/boxcount/html/demo.html

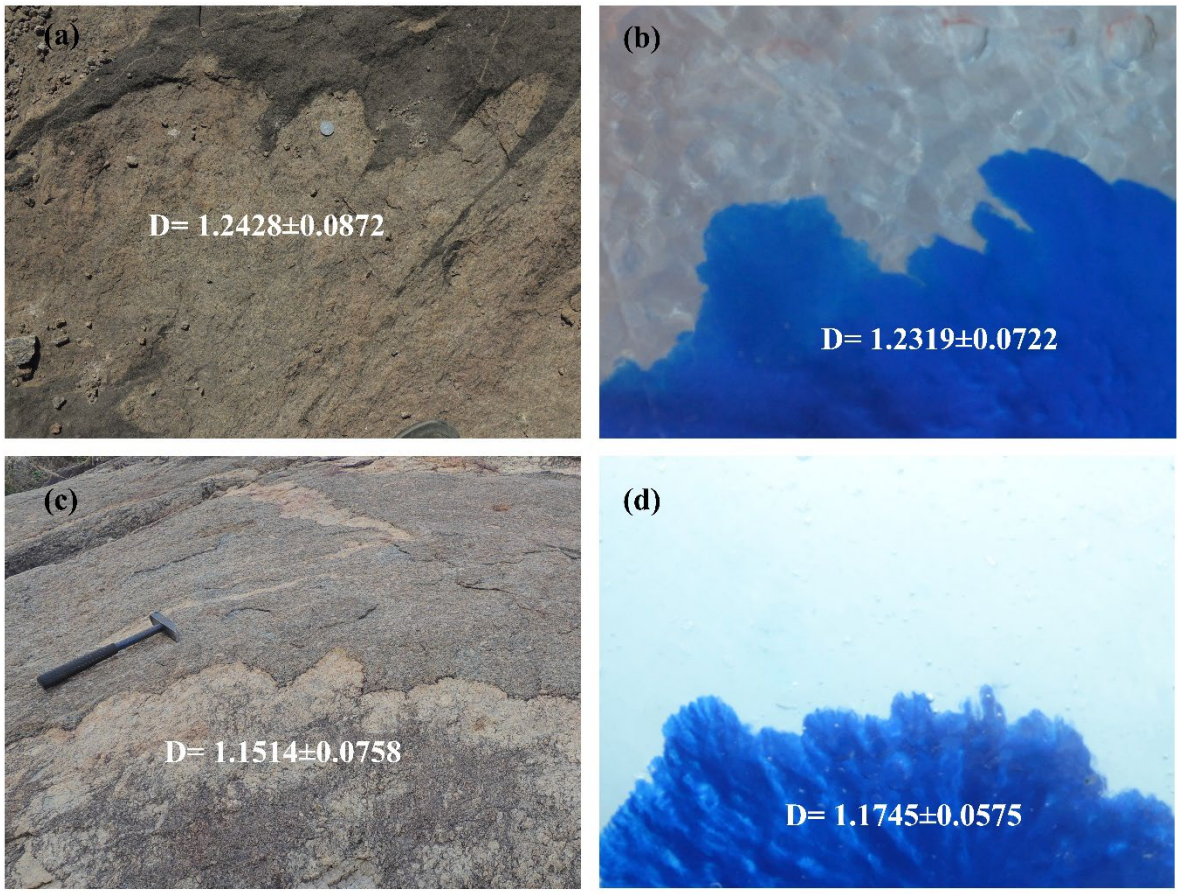

Figure S12. Matching fractal dimensions were found for both the field sample (*left column*) and experimental models (*right column*).

The procedure of Aspect Ratio Calculation S5.

To calculate the aspect ratio (a) of a protrusion, we measured the half wavelength (L) and the amplitude (H) using CorelDraw 2021, as shown in Figure S13. The collected data is provided in the data depository. (Biswas et al., 2023). The measured values do not represent the real scale. However, they are carefully measured from an undistorted photograph. As the a is a calculation of the ratio of L and H, the scale of measurement does not affect the value.

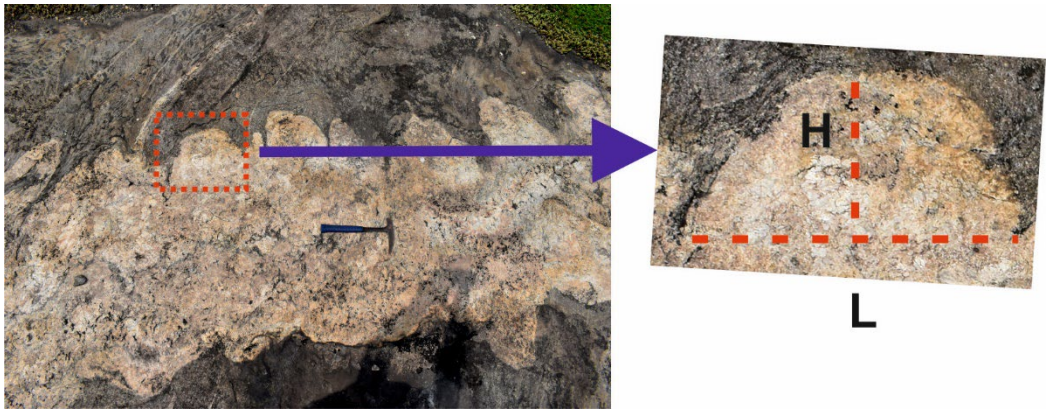

191

192 **Figure S13.** The procedure of Aspect Ratio (*a*) calculations

193 **The procedure of Skewness and Kurtosis Calculation S6.**

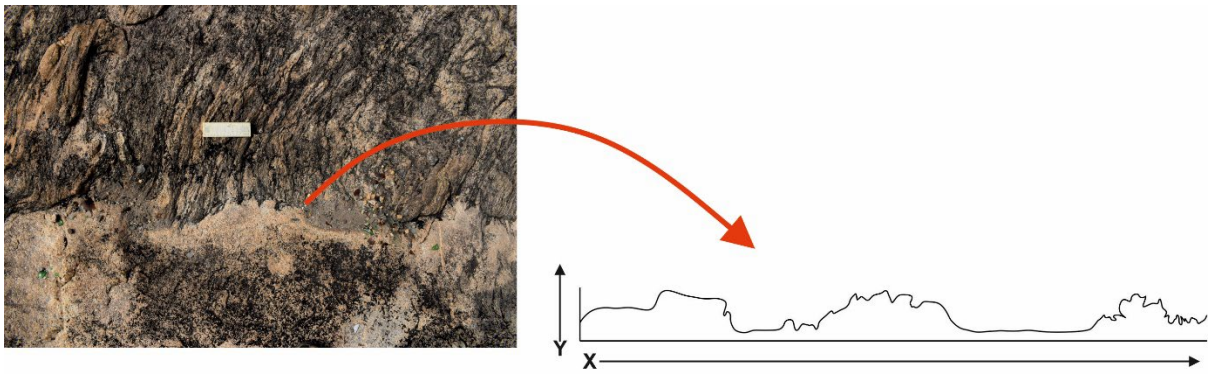

194

195 **Figure S14.** The boundary between the host and the intrusion was reconstructed using MATLAB for
196 skewness-kurtosis calculations.

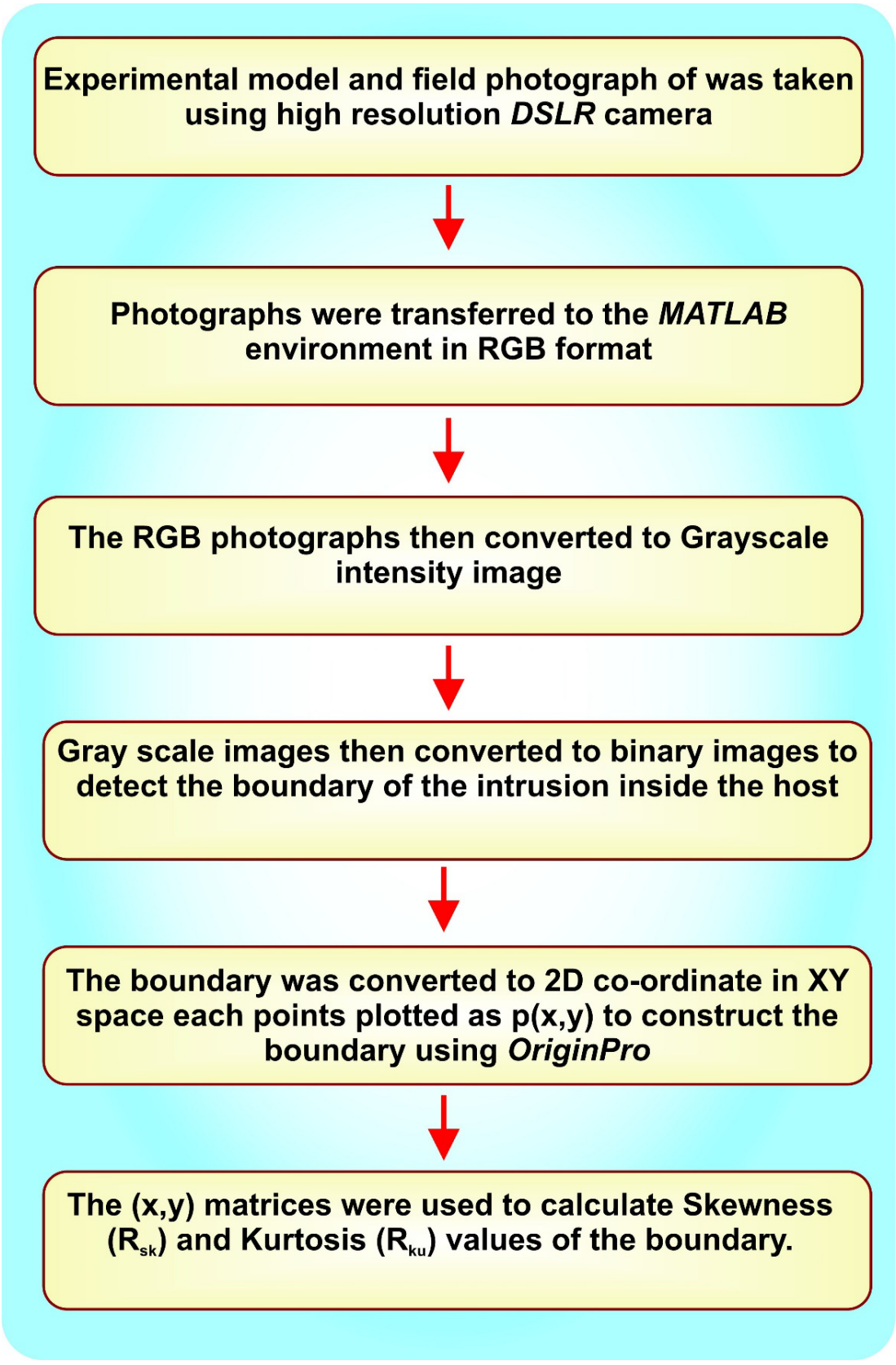

197

198 **Figure S15.** Flow chart of the procedure steps for calculations of skewness and kurtosis of irregular
199 intrusion boundaries.

200

Supplementary Figures S7

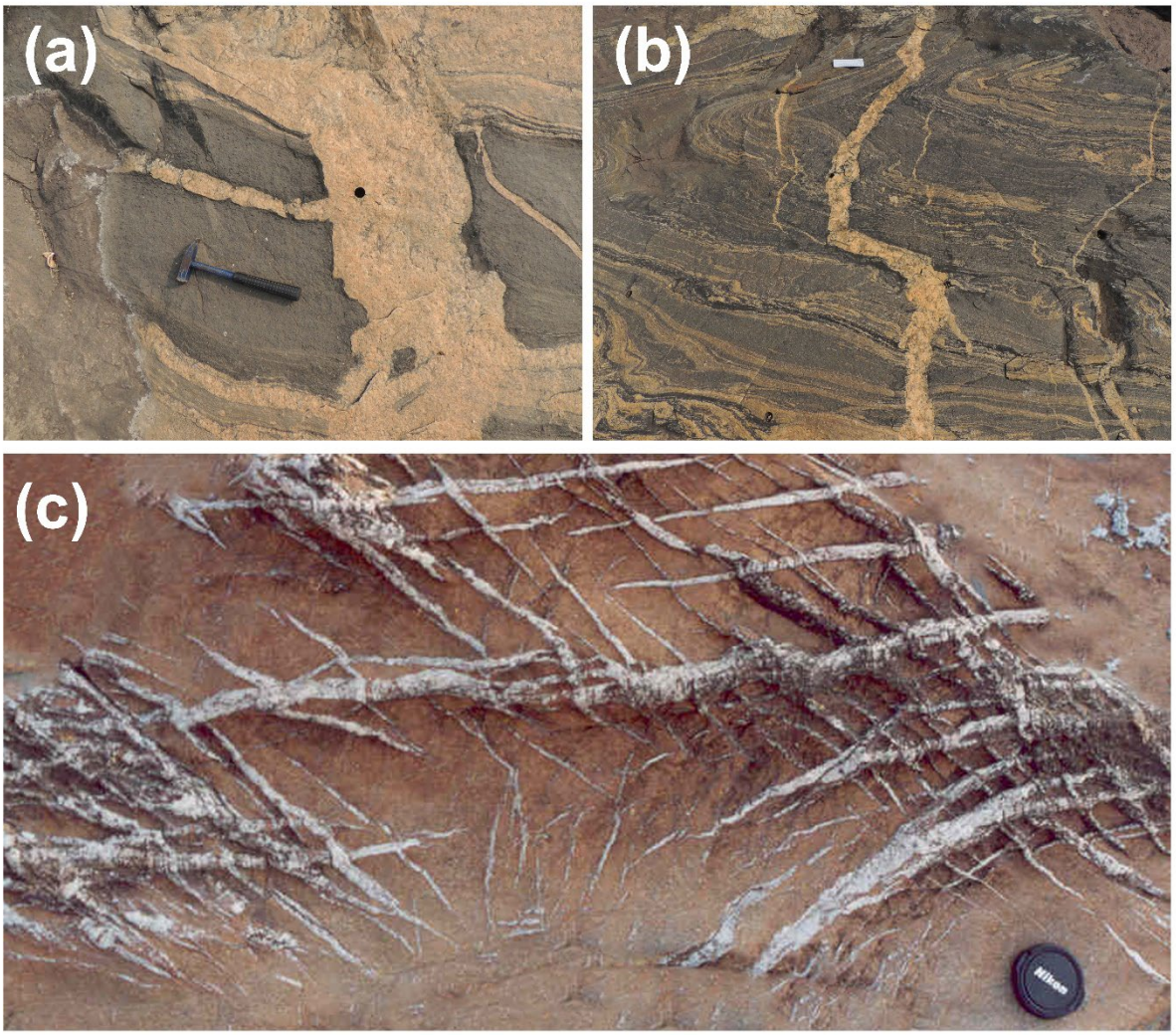

Figure S16. (a) Dike in CGGC showing branching at a very high angle (~90°), (b) Sharp boundary pure fracture dominated dike in the field, Purulia, West Bengal., and (c) Networking of small-scale dikes in the field.

References

- Birren, T., Reber, J.E., 2019. The impact of rheology on the transition from stick-slip to creep in a semi-brittle analog. J. Geophys. Res. Solid Earth 124 (3), 3144–3154.
- Canon-Tapia, E., Merle, O., 2006. Dyke nucleation and early growth from pressurized magma chambers: Insights from analog models. J. Volcanol. Geotherm. Res. 158 (3–4), 207–220.
- Hayman, N.W., Ducloue, L., Foco, K.L., Daniels, K.E., 2011. Granular controls on periodicity of stick-slip events: kinematics and force-chains in an experimental fault. Pure Appl. Geophys. 168 (12), 2239–2257.
- Hubbert, M.K., Theory of scale models as applied to the study of geologic structures, Geol. Soc. Amer. Bull. 48 (1937) 1459–1520.

- Kervyn, M., Ernst, G.G.J., de Vries, B.V., Mathieu, L., Jacobs, P., 2009. Volcano load control on dyke propagation and vent distribution: Insights from analog modeling. J. Geophys. Res. Solid Earth 114.
- Mezger, T.G., The Rheology Handbook, Vincentz Network, Hanover, Germany, 2014, ISBN 978-3-86630-650-9
- Oppong, F.K., de Bruyn, J.R., 2011. Microrheology and jamming in a yield-stress fluid. Rheol. Acta 50 (4), 317–326.
- Piau, J.M., 2007. Carbopol gels: Elastoviscoplastic and slippery glasses made of individual swollen sponges Meso- and macroscopic properties, constitutive equations, and scaling laws. J. Non-Newtonian Fluid Mech. 144 (1), 1–29.
- Ramberg, H., Gravity, deformation and the Earth's crust, Academic Press, New York, 1981, 452 pp.
- Reber, J. E., Cooke, M. L., & Dooley, T. P. (2020). What model material to use? A Review on rock analogs for structural geology and tectonics. Earth-Science Reviews, 202, 103107.
- Reber, J.E., Lavier, L.L., Hayman, N.W., 2015. Experimental demonstration of a semi-brittle origin for crustal strain transients. Nat. Geosci. 8 (9), 712.
- Rivalta, E., Bottinger, M., Dahm, T., 2005. Buoyancy-driven fracture ascent: Experiments in layered gelatine. J. Volcanol. Geotherm. Res. 144 (1–4), 273–285.
- Rubin, A. (1993). Dikes vs. diapirs in viscoelastic rock. Earth Planet. Sci. Lett. 119, 641–659.
- Scheibert, J., Galland, O., and Hafver, A. (2017). Inelastic deformation during sill and laccolith emplacement: insights from an analytic elastoplastic model. J. Geophys. Res. Solid Earth 122, 923–945. doi: 10.1002/2016JB013754
- Shafiei, M., Balhoff, M., Hayman, N.W., 2018. Chemical and microstructural controls on viscoplasticity in Carbopol hydrogel. Polymer 139, 44–51.
- Vachon, R., and Hieronymus, C. F. (2016). Effect of host-rock rheology on dike shape, thickness, and magma overpressure. Geophys. J. Int. 208, 1414–1429. doi: 10.1093/gji/ggw448